Available online at www.sciencedirect.com
SCIENCE DIRECT®
Catalysis Today 90 (2004) 297–303
CATALYSIS TODAY
www.elsevier.com/locate/cattod

Adsorption and photocatalytic decomposition of methylene blue on mesoporous metallosilicates

Isamu Moriguchi [a,*], Masakuni Honda [a], Taro Ohkubo [a], Yoshio Mawatari [a], Yasutake Teraoka [b]

[a] *Department of Applied Chemistry, Faculty of Engineering, Nagasaki University, Nagasaki 852-8521, Japan*
[b] *Department of Material Sciences, Faculty of Engineering Sciences, Kyushu University, Kasuga, Fukuoka 816-8580, Japan*

Abstract

Mesoporous silica and mesoporous metallosilicates with Al, Ti and Fe as foreign metal species were successfully synthesized by the rapid room temperature method. Mesoporous metallosilicates with low contents of foreign metals possessed high surface area (S_a), large mesopore volume (V_{mp}) and highly ordered hexagonal mesoporous structure. Increases in foreign metal contents caused disordering the mesoporous structures and lowering the S_a and V_{mp} values. Bleaching of aqueous methylene blue (MB) by mesoporous silica and metallosilicates was investigated. Mesoporous aluminosilicate and ferrosilicate with cation-exchangeable ability showed the excellent property for the adsorption of MB of cationic dye, while mesoporous ferrosilicate and titanosilicate which absorbed UV lights catalyzed the photocatalytic decomposition of MB under UV-illumination.

Keywords: Mesoporous; Metallosilicate; Methylene blue; Adsorption; Photocatalysis

1. Introduction

Synthesis and application of mesoporous materials is currently the subject of intensive research in materials sciences because of their prominent features such as high surface area (above $1000\,m^2\,g^{-1}$ for silica), narrow pore size distribution in mesopore region and highly ordered mesopore arrangements. A lot of self-assembly systems of surfactants and amphiphilic block copolymers have been employed to direct the mesoporous structures of not only silica but also non-silica metal oxides [1–5]. For the templating synthesis, hydrothermal processes under alkaline conditions are mostly adopted as suitable synthetic conditions. In contrast, a few studies refereed to the synthesis under an acidic and room temperature condition as a convenient (shorter synthetic time, non-heating to yield mesostructured precursor) and low-cost method for yielding mesoporous silica [6,7]. We have so far studied a rapid room temperature (RRT) process using aqueous silicate source such as sodium silicate [7]. It has been found that ordered hexagonal mesostructures of the surfactant/silicate precursor are produced within a few hours from strongly acidic to basic pH conditions ($0 \leq pH < 11$) and the precursor can be converted into high quality mesoporous silica with high surface area above $1000\,m^2\,g^{-1}$ by an air-calcination [7].

Considering the application of mesoporous materials to adsorbents or catalysts, it is desirable to introduce active sites in the mesopore wall or on the mesopore surface. In this respect, the synthesis of mesoporous materials of metallosilicates would contribute to design and develop novel adsorbents and catalysts. The adaptability of the RRT process in wide-ranging pH have been proved to be useful for synthesis of various metallosilicates because the pH value should be adjusted to the values specific to foreign metal species in the synthetic solutions [8]. In the present paper, mesoporous metallosilicates with Al, Fe and Ti as foreign metals were synthesized by the RRT process, and adsorption and photocatalytic decomposition of methylene blue (MB) on the mesoporous metallosilicates were investigated.

* Corresponding author. Tel.: +81-95-819-2669; fax: +81-95-819-2669.
E-mail address: mrgch@net.nagasaki-u.ac.jp (I. Moriguchi).

0920-5861/$ – see front matter © 2004 Elsevier B.V. All rights reserved.
doi:10.1016/j.cattod.2004.04.034

2. Experimental

2.1. Synthesis of mesoporous silicates

The chemical reagents used for the synthesis, sodium silicate ($Na_2O{\cdot}2SiO_2{\cdot}2.52H_2O$, chemical use grade), sodium alminate ($NaAlO_2$, 70% chemical use grade), titanium butoxide ($Ti(OBu)_4$, extra pure grade), iron sulfate 14-hydrate ($Fe_2(SO_4)_3{\cdot}14H_2O$, 99% guaranteed grade), cetylpyridinium chloride mono-hydrate ($C_{16}PyCl{\cdot}H_2O$, 95% extra pure grade), sodium hydroxide (NaOH, 96% guaranteed grade) and hydrochloric acid (35% HCl, guaranteed grade), were of Kishida Co. Ltd.

The $C_{16}PyCl$ surfactant was added into 50 mL of water, and this solution was vigorously stirred with optional heating in order to obtain a clear micelle solution. An aqueous solution of the foreign metal source (Me = Al, Fe, Ti) was dropwise added to the micelle solution whose pH value had been adjusted with conc. HCl and aq. NaOH, and then a clear aqueous solution of sodium silicate (250 mmol in 5 mL of water) was added under vigorous stirring. The molar ratio of $C_{16}Py/(Si + Me)$ was set at 0.12. After further stirring for 3 h at room temperature, the obtained precipitates were washed with water, dried at 385 K for 3 h and calcined at 823 K for 6 h. The appropriate pH values after adding the Si source solution differed depending on the kind and content of foreign metal species, and they were listed in Table 1. In the following, the samples were referred to as Meso-MeSi-*x*, where Me is the foreign metal species (Al, Fe and Ti) and *x* is the Si/Me ratio charged in the synthetic condition. Mesoporous silica (Meso-Si) was synthesized by the same method without the addition of the solution of foreign metal sources.

2.2. Characterization

X-ray powder diffraction (XRD) patterns were obtained on a Rigaku LINT2200 diffractometer using Cu Kα radiation. Adsorption–desorption isotherms of N_2 were measured at 77 K (Micromeritics Co. Ltd. Gemini 2370). The specific surface area and mesopore diameter distribution were, respectively, analyzed by BET and BJH methods from the N_2 adsorption branch. Diffuse reflectance (DR) UV-Vis spectra were recorded at room temperature on a Shimadzu UV-3100 spectrometer equipped with an integrating sphere using $BaSO_4$ as a reference material; the data were processed according to Kubelka–Munk theory. Metal compositions of the products were analyzed by atomic absorption analysis (Shimadzu AA-640-12) after they were dissolved in aqueous HF. IR and ESR spectra were recorded at room temperature on Perkin-Elmer 1650 (KBr method) and JEOL JES-FE1XG, respectively.

2.3. Bleaching of aqueous dye solutions

Methylene blue (MB) and Orange II were purchased from Wako Pure Chemical Co. Ltd. Typical experimental procedures using MB were as follows. Bleaching of aqueous MB was carried out at 298 K in a thermocontrolled batch reactor (250 ml of 5.0×10^{-5} mol dm^{-3} aqueous MB, pH 6.6) with or without illumination using 100 W Hg lamp (Ushio UM-102), to which 50 or 25 mg of mesoporous metallosilicate powder was suspended and air was introduced through a bubbler. With intervals of 10–60 min, a small portion of the reaction solution was separated and the dye concentration was measured by UV-Vis spectroscopy (Shimadzu MultiSpec-1500) using absorbance at 665 and 485 nm for

Table 1
Characterization of mesoporous silica (Meso-Si) and metallosilicates (Meso-MeSi, Me = Al, Fe, Ti)

Meso-MeSi	*x* (Si/Me)[a]	pH[b]	Observed Si/Me[c]	S_a ($m^2\,g^{-1}$)[d]	V_{mp} ($cm^3\,g^{-1}$)[e]	D_{mp} (Å)[f]
Meso-Si	∞	<1	∞	1198	0.85	24
Meso-AlSi	49	10.8	39.0	1120	0.91	26
	20	10.8	15.0	1156	0.83	25
	10	10.8	10.3	939	0.60	24
	5	10.8	6.7	779	0.45	23
Meso-FeSi	75	11.4	33.2	1093	0.78	26
	49	11.2	19.9	926	0.64	25
	15	10.7	13.8	799	0.46	23
	8	9.5	8.0	793	0.36	20
Meso-TiSi	38	<1	–	1641	1.36	24
	18	<1	–	1647	1.22	22
	10	<1	–	1162	0.72	20
	5	<1	–	1052	0.46	18

[a] The molar ratio of Si/Me charged in the synthetic solution.
[b] pH of solution after adding Si source.
[c] Determined by atomic absorption analysis.
[d] Specific surface area.
[e] Mesopore volume.
[f] Mean mesopore diameter calculated by BJH method.

MB and Orange II, respectively. The measurements were also performed on silica gel (JRC-SIO-5, Catalysis Society of Japan) and MFI (silica/alumina = 39.5, Tosoh Co.).

3. Results and discussion

3.1. Synthesis of mesoporous metallosilicates (MPMSs)

Fig. 1 shows the XRD patterns of mesoporous silica (Meso-Si) and mesoporous aluminosilicate (Meso-AlSi) synthesized by the RRT process. Meso-AlSi-49 showed a distinct XRD pattern assignable to the hexagonal array of mesopores as similar to that of Meso-Si. With increasing the Al content (decreasing x), the orderliness of the hexagonally arrayed structure decreased, as evidenced by weakening and broadening of the strongest (1 0 0) peak. As shown in Fig. 2, however, all the Meso-AlSi prepared here showed the inflection characteristics of capillary condensation into mesopores at $0.2 < p/p_0 < 0.3$ in nitrogen adsorption isotherms, confirming the formation of mesoporous materials with pore diameters between 22 and 25 Å. The specific surface area (S_a) and mesopore volume (V_{mp}) decreased with increasing the Al content, but Meso-AlSi-x with $x = 20$ possessed large values of S_a and V_{mp} comparable to those of Meso-Si (Table 1). Although the Si/Al ratios observed slightly deviated from the charged ratios in the synthesis (x), the almost linear relation was observed between the observed and charged Si/Al ratios, indicating that the Si/Al ratio in Meso-AlSi can be controlled by x in the starting solution. It was revealed that Meso-AlSi exhibited an ion-exchange property and that the almost all Al in Meso-AlSi were present in tetrahedrally coordinated sites as evidenced by ^{27}Al MAS NMR [8,9]. These results indicate that Al ions are substitutionally incorporated in the silicate framework.

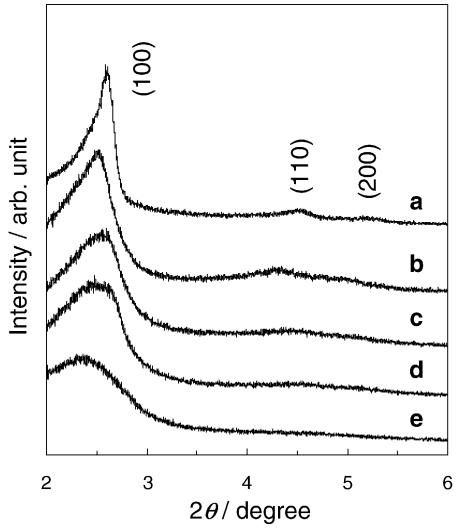

Fig. 1. XRD patterns of Meso-Si and Meso-AlSi-x: (a) Meso-Si; (b) Meso-AlSi-49; (c) Meso-AlSi-20; (d) Meso-AlSi-10; (e) Meso-AlSi-5.

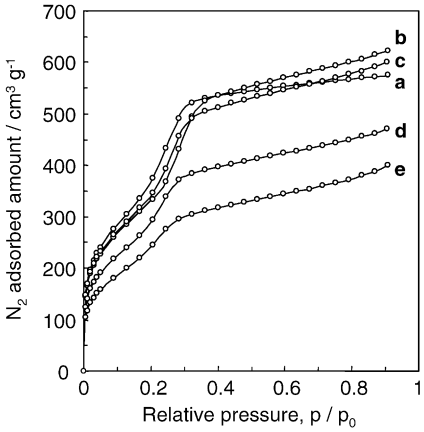

Fig. 2. Nitrogen adsorption isotherms of Meso-Si and Meso-AlSi. (a)–(e) are the same as in Fig. 1. Only adsorption branches are shown because no apparent hysteresis was observed.

Mesoporous ferrosilicates (Meso-FeSi) with Si/Fe ratios above 8.0 were successfully obtained in the pH range of $9.5 < \text{pH} < 11.4$ as listed in Table 1. The Meso-FeSi clearly showed the capillary condensation into mesopores in nitrogen adsorption isotherms (Fig. 3), although the hexagonal arrangement of mesopores is not so well ordered as can be seen from Fig. 4. It should be stated that any XRD peaks assignable to iron oxides were not observed for all the samples synthesized. As in the case of Meso-AlSi, the S_a and V_{mp} values of Meso-FeSi-x decreased with decreasing x (increasing Fe content) and the samples with low Fe content (Meso-FeSi-75, −49) have relatively high surface area close to 1000 $m^2\,g^{-1}$. Meso-FeSi showed UV absorption around 260 nm probably due to tetrahedrally coordinated Fe(III) species and the absorbance increased with increasing Fe content. An IR band assignable to Si–O–Fe symmetric stretching [10,11] was observed at around 675 cm^{-1} for Meso-FeSi. In addition, Meso-FeSi showed ESR signals at

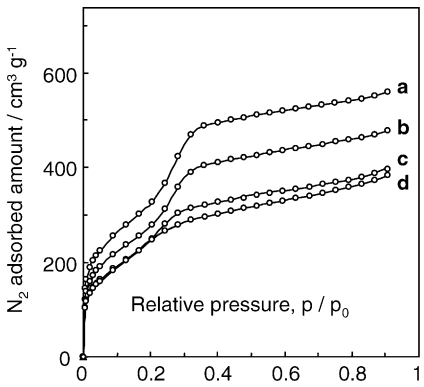

Fig. 3. Nitrogen adsorption isotherms of Meso-FeSi-x with (a) $x = 75$, (b) $x = 49$, (c) $x = 15$ and (d) $x = 8$. Only adsorption branches are shown because of no apparent hysteresis was observed.

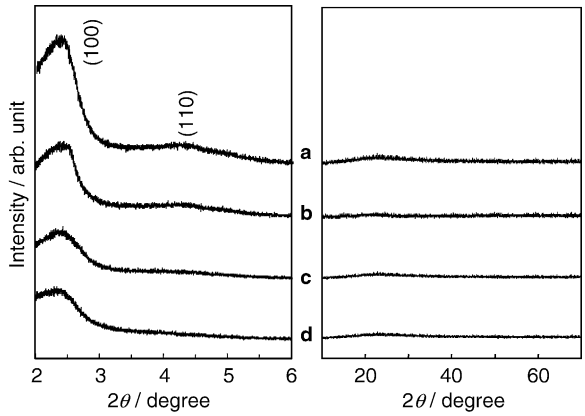

Fig. 4. XRD patterns of Meso-FeSi-*x*. (a)–(d) are the same as in Fig. 3.

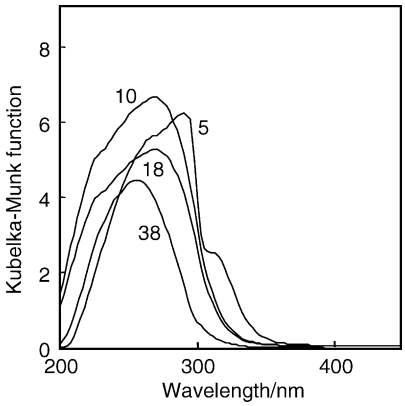

Fig. 6. Diffuse reflectance spectra of Meso-TiSi-*x*. The numeral in figure indicates *x*.

$g = 4.3$ and 1.99 (Fig. 5), which are assignable to trivalent irons in symmetrical tetrahedral and distorted tetrahedral coordinations, respectively [12,13]. The relative intensity of the latter increased with increasing the charged Fe content. These results indicate that Fe ions are substitutionally incorporated in the silicate framework with the tetrahedral coordination and that the increase in the Fe content causes a distortion of the coordination symmetry and disordering the mesoporous structure.

Mesoporous titanosilicates (Meso-TiSi) possessed surface areas higher than those of Meso-AlSi and Meso-FeSi, and the S_a and V_{mp} values decreased with decreasing x as similar to Meso-AlSi and Meso-FeSi (Table 1). As we reported previously [7], the S_a value of Meso-Si synthesized by the RRT process tended to decrease with increasing the pH of the solution. Therefore, Meso-TiSi synthesized in the acidic condition showed higher S_a value than Meso-AlSi and Meso-FeSi synthesized in the basic condition. In addition, since the S_a value of mesoporous silicates synthesized in highly acidic condition (pH < 1) was widely ranging usually between 1200 and 1600 $m^2\,g^{-1}$ and it was not easy to control the S_a value, Meso-Si and Meso-TiSi had different specific surface even though they were synthesized in the highly acidic condition. In UV-Vis spectra, Meso-TiSi-*x* with $x = 38$, 18 and 10 showed absorption below 300 nm with a peak maximum around 250–275 nm and a shoulder peak around 220 nm (Fig. 6). The peak maximum tended to shift toward longer wavelength with decreasing *x*. For Meso-TiSi-5, an additional UV absorption was observed at 300–350 nm accompanied with the UV absorption below 300 nm. It is reported that the isolated Ti(IV) species with tetragonal coordination in silicate framework shows UV absorption around 220 nm due to a charge transfer between framework oxygen and tetrahedral Ti(IV) and the absorption above 220 nm appeared when the coordination of Ti(IV) changes to the octahedral one by the insertion of water molecules as extra ligands [14,15]. Thus, it is inferred that tetragonal and octahedral Ti species coexisted in the mesoporous framework of Meso-TiSi-*x* with $x \leq 10$ and the octahedral one increased with decreasing *x*. The UV absorption at 300–350 nm observed for Meso-TiSi-5 might indicate the presence of TiO_2 nanoparticles out of the framework.

From these results, it can be concluded that the wide-ranging pH-allowance of the RRT process in the mesoporous silica synthesis has made it possible to synthesize various mesoporous metallosilicates if the pH value and the charged Si/Me ratio in the synthetic solution have been adjusted to the values specific to foreign metal species.

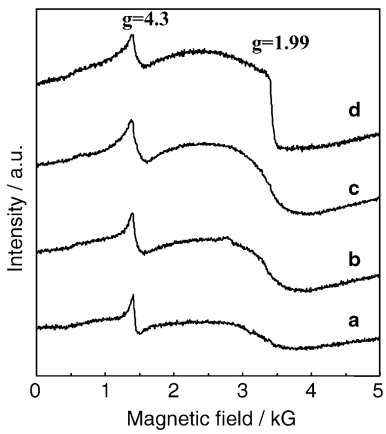

Fig. 5. ESR spectra of Meso-FeSi-*x*. (a)–(d) are the same as in Fig. 3.

3.2. Adsorption of methylene blue on mesoporous metallosilicates

Fig. 7 shows the time courses of the MB removal from the aqueous systems (pH 6.6) dispersing mesoporous silicates (Meso-Si, Meso-AlSi-50, Meso-FeSi-49, Meso-TiSi-18) and silica gel under the dark condition (unillumination). With passing time, the amount of MB removed from the liquid phase increases, and leveled off above 1–3 h. Since the dispersed solids were colored blue with passing time, the removal of MB is due to the adsorption of MB molecules on the porous solids from the aqueous phase. The adsorbed

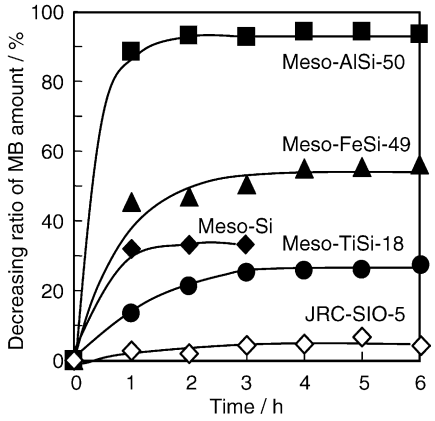

Fig. 7. Time courses of MB removal from aqueous solution (dark reaction); 50 mg of adsorbents was dispersed in 250 mL of aqueous MB (5.0×10^{-5} mol dm^{-3}, pH 6.6).

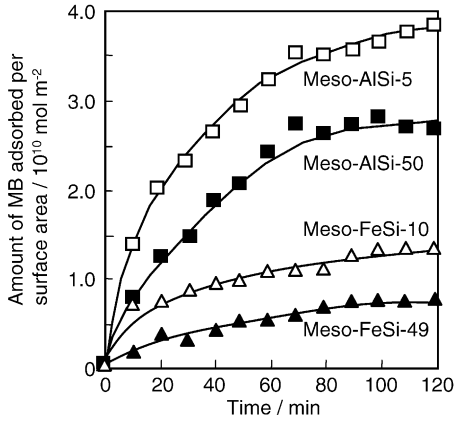

Fig. 9. Time courses of adsorbed MB amount on Meso-AlSi-*x* and Meso-FeSi-*x* (dark reaction); 25 mg of Meso-MeSi was dispersed in 250 mL of aqueous MB (5.0×10^{-5} mol dm^{-3}, pH 6.6).

amount of MB per weight of the adsorbent decreased in the order of Meso-AlSi-50 > Meso-FeSi-49 > Meso-Si > Meso-TiSi-18 > silica gel. The amount of MB adsorbed per unit surface area of the adsorbents was followed Meso-AlSi-50 > Meso-FeSi-49 > Meso-Si > silica gel ≈ Meso-TiSi-18 (Fig. 8). The larger MB amount adsorbed on Meso-Si than on silica gel suggests that mesopores with diameter of 24 Å are effective to the adsorption of MB with ca. 15 Å molecular size; the multi-point interaction between silica surface (wall) and MB is expected when the molecular and mesopore sizes are close. The MB adsorption amount on the MFI zeolite was far lower than those on Meso-Si and silica gel because its pore size (4.5 Å) is too small to incorporate MB molecules.

Results on the removal of MB by adsorption (Figs. 7 and 8) show that the incorporation of Al and Fe into the mesoporous silicate framework is effective to the adsorption of MB, which is a cationic dye. The effectiveness of incorporating Al and Fe was also demonstrated in the experiments

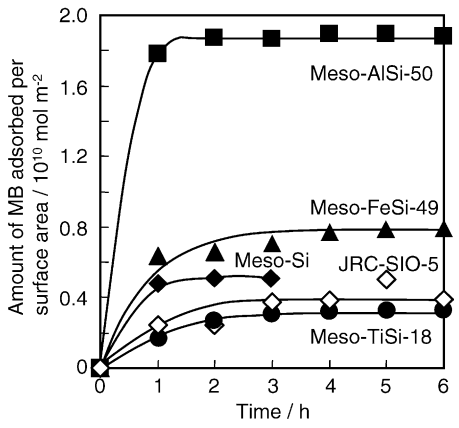

Fig. 8. Time courses of adsorbed MB amount per surface area of adsorbents calculated from the results of Fig. 7 and specific surface areas of the adsorbents.

that the MB-adsorbed amount increased with increasing Al and Fe content (decreasing *x*) for Meso-AlSi and Meso-FeSi (Fig. 9). The adsorption isotherms of MB (MB adsorption amount versus equilibrium concentration of aq. MB) on Meso-AlSi-10, Meso-FeSi-15 and Meso-Si were measured at pH 6.6. They fit well with the Langmuir isotherm and the calculated equilibrium constant, *K*, and maximum adsorption amount per unit surface area, V_M, were listed in Table 2. The values of *K* and V_M of Meso-AlSi-10 and Meso-FeSi-15 are obviously larger than those of Meso-Si, confirming again the superior adsorption property of the Al- and Fe-incorporated systems to pure silica mesoporous material. As we already reported, cation-exchangeable sites are generated when trivalent Al is substitutionally incorporated in the mesoporous silicate framework [7]. Since Fe in Meso-FeSi takes trivalent and is substitutionally incorporated in the tetrahedrally coordination sites as stated above, it is expected that the cation-exchangeable sites would be generated also in the Meso-FeSi. Considering the inferior MB adsorption property of Meso-TiSi in which the generation of the cation-exchangeable sites is hardly expected by the substitution of Ti^{4+} for Si^{4+}, it is concluded that the cation-exchangeable property of mesoporous metallosilicates is primarily responsible for the adsorption of cationic MB. Calculation from the observed Al content and V_M value of Meso-Al-Si-10, for example, shows that about 60% of the

Table 2
Langmuir parameters of the adsorption of MB on mesoporous materials

Mesoporous material	pH of aq. MB	*K* (m^3 mol^{-1})[a]	V_M (μmol m^{-2}-solid)[b]
Meso-AlSi-10	6.6	1.05×10^3	0.42
Meso-FeSi-15	6.6	0.30×10^3	0.34
Meso-Si	6.6	0.15×10^3	0.09
Meso-Si	8.6	0.25×10^3	0.20

[a] Equilibrium constant.
[b] Maximum adsorption amount per unit surface area.

incorporated Al contributes to the MB adsorption through the electrostatic interaction if all of introducing Al forms ion-exchange sites on the surface. The importance of the cation-exchangeable property on the MB adsorption was also confirmed by the following experiments:

- The adsorption amount of the anionic Orange II dye molecules was negligibly small for Meso-AlSi and Meso-FeSi.
- As shown in Table 2, the adsorption property (K and V_M) of Meso-Si at pH 8.6 was higher than that at pH 6.6. This can be explained by the electrostatic interaction of cationic MB and negatively charged Meso-Si surface. If we consider that the value of isoelectric point (IEP) of Meso-Si is close to that of silica gel (1.8–2.5) [16], the surface of Meso-Si is negatively charged above IEP and the surface density of the negative charge increases with increasing pH.
- The similar pH dependence was also observed with Meso-TiSi, the IEP of which was estimated to be around 3.5 from a pH titration experiments. The elevation of IEP by the incorporation of Ti causes the decrease in the surface negative charge density at a pH value of MB adsorption, 6.6, for example, as compared with Meso-Si. This might be a reason why the MB adsorption property of Meso-TiSi is slightly inferior to that of Meso-Si.

3.3. Photocatalytic decomposition of methylene blue on mesoporous metallosilicates

Fig. 10 shows the time courses of the MB removal under UV-illumination in the aqueous dispersion systems (pH 6.6) of mesoporous silicates (Meso-Si, Meso-AlSi-50, Meso-FeSi-49, Meso-TiSi-18) and silica gel. Compared with Fig. 7 (dark reaction), an enhancement of the MB removal by the UV-illumination was observed on Meso-FeSi-49 and Meso-TiSi-18, and they were not colored blue even after the UV-illumination for a few hours. In contrast, UV-illumination had little effect on the MB removal with Meso-AlSi-50, Meso-Si and silica gel, and they became colored blue with passing reaction time. These results indicate that photocatalytic decomposition of MB takes place on Meso-FeSi and Meso-TiSi which absorb UV light as described above.

As stated in Section 3.2, mesoporous metallosilicates have adsorption property against MB in the dark condition. Therefore, it is difficult to evaluate the neat photocatalytic activity from the time course of MB removal. Here, the difference of the MB removal between the UV-illuminated and dark conditions (Δ[UV − dark]) is used as an apparent measure to evaluate the impact of the UV-illumination on the MB removal. Actually, this is not the real parameter to evaluate the photocatalytic activity because all the MB molecules removed were photocatalytically decomposed after adsorption on Meso-FeSi and Meso-TiSi. Even under such a circumstance, the parameter of Δ[UV − dark] might be used to compare the impact of the UV-illumination between samples.

In the Meso-FeSi system (Fig. 11), the Δ[UV − dark] values leveled off after 2 h because almost all MB were removed until 3 h. The higher contribution of photodecomposition in Meso-FeSi-10 than in Meso-FeSi-49 clearly suggests that the incorporated Fe species act as photocatalytic active sites. The results on Meso-TiSi (Fig. 12) were complicated but could be understood if both the adsorption and the photocatalytic decomposition were taken into account. The adsorption effect on the MB photodecomposition was clearly observed on the measurements in aqueous MB at pH 6.6 (curve d) and 8.6 (curve a) with Meso-TiSi-38. As stated above, the amount of MB adsorbed increased by changing the pH value from 6.6 to 8.6. The increased adsorption amounts should result in the enhancement of the photodecomposition of MB, because the photoactivated catalytic active site decomposes the MB adsorbed on or near it. It is noted that 90–100% removal of MB from the aqueous phase of pH 8.6 was accomplished with Meso-TiSi-38 within 3 h under the UV-illumination, being in contrast to the 45%

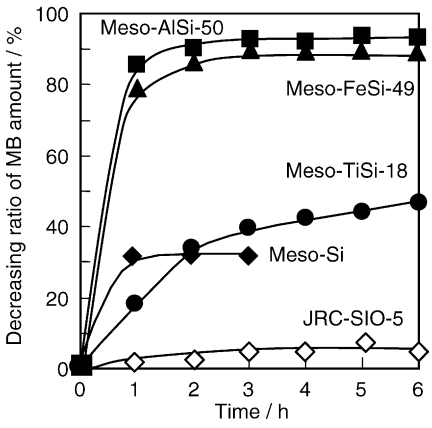

Fig. 10. Time courses of MB removal from aqueous solution under UV-illumination; the solution condition is the same as in Fig. 7.

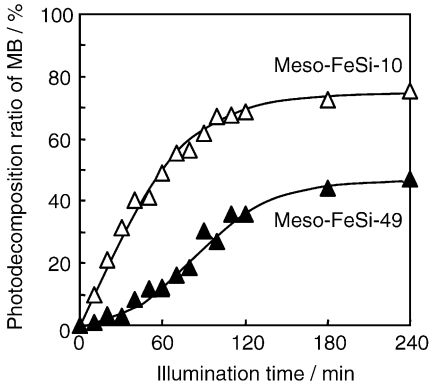

Fig. 11. Time courses of apparently photodecomposed MB, Δ[UV − dark], on Meso-FeSi-10 and Meso-FeSi-49; 25 mg of Meso-FeSi was dispersed in 250 mL of aqueous MB (5.0×10^{-5} mol dm^{-3}, pH 6.6). See text for the definition of Δ[UV − dark].

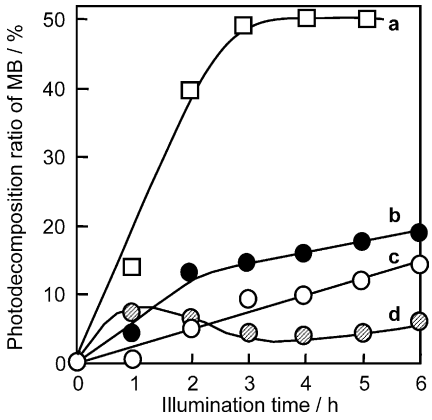

Fig. 12. Time courses of apparently photodecomposed MB, Δ[UV−dark], on Meso-TiSi-*x* ($x = 5$, 18, 38); 50 mg of Meso-TiSi was dispersed in 250 mL of aqueous MB (5.0×10^{-5} mol dm^{-3}, pH = 6.6, 8.6). (a) $x = 38$ (pH 8.6), (b) $x = 18$ (pH 6.6), (c) $x = 5$ (pH 6.6), (d) $x = 38$ (pH 6.6).

removal under the dark condition. The dependence of the photodecomposition on the Ti content measured at pH 6.6 can be explained separately in the initial (<2 h) and steady (>3 h) stages. At the steady stage, Δ[UV − dark] increased linearly with illumination time, and the slope corresponding to the apparent photodecomposition rate increased as Meso-TiSi-38 < Meso-TiSi-18 < Meso-TiSi-5. The result that the apparent rate increased with increasing Ti content suggests that Ti incorporated in the silicate framework serves as an active photodecomposition sites and that the inherent photocatalytic activity is primarily responsible at the steady stage. Within 1 h under illumination, the apparent amount of MB photocatalytically removed changed as Meso-TiSi-5 < Meso-TiSi-18 < Meso-TiSi-38 which is the completely reverse of the order in the steady stage. As stated above, the amount of MB adsorbed increased as the same order of the apparent photocatalytic removal of MB. Therefore, the adsorption ability of Meso-TiSi against MB might be more important in the initial stage than the inherent photocatalytic activity. The real photocatalytic property of Meso-FeSi and Meso-TiSi should be revealed by further investigation.

Acknowledgements

The study made use of the XRD diffractometer in the Center for Instruments Analysis of Nagasaki University.

References

[1] C.T. Kresge, M.E. Leonowicz, W.J. Roth, J.C. Vartuli, J.B. Beck, Nature 359 (1992) 710.
[2] P. Yang, D. Zhao, D. Margolese, B.F. Chmelka, G.D. Stucky, Chem. Mater. 11 (1999) 2813.
[3] B.T. Holland, C.F. Blanford, T.A. Stein, Chem. Mater. 11 (1999) 795.
[4] S. Biz, M.L. Occelli, Catal. Rev. Sci. Eng. 40 (1998) 329.
[5] B. Lee, D. Lu, J.N. Kondo, K. Domen, J. Am. Chem. Soc. 124 (2002) 11256.
[6] Q. Huo, D.L. Margolese, U. Ciesla, P. Feng, T.E. Gier, P. Sieger, R. Leon, P.M. Petroff, F. Shuthe, G.D. Stucky, Nature 368 (1994) 317.
[7] Y.M. Setoguchi, Y. Teraoka, I. Moriguchi, S. Kagawa, N. Tomonaga, A. Yasutake, J. Izumi, J. Por. Mater. 4 (1997) 129;
Y. Teraoka, I. Moriguchi, S. Kagawa, Adsorpt. News 12 (1999) 6 (in Japanese).
[8] Y. Teraoka, Y.M. Setoguchi, K. Ideguchi, I. Moriguchi, S. Kagawa, N. Tomonaga, A. Yasutake, J. Izumi, in: Proceedings of Fundamentals of Adsorption 7, IK International Ltd., 2002, p. 208.
[9] Y. Teraoka, Y. Fukunaga, Y.M. Setoguchi, I. Moriguchi, S. Kagawa, N. Tomonaga, A. Yasutake, J. Izumi, in: Proceedings of the Second Pacific Basin Conference on Adsorption Science and Technology, World Scientific, Singapore, 2000, p. 603.
[10] S.K. Badamali, A. Sakthivel, P. Selvam, Catal. Lett. 65 (2000) 153.
[11] S. Bordiga, R. Buzzoni, F. Geobaldo, G. Lamberti, E. Giamello, A. Zeccina, G. Leofanti, G. Pertrini, G. Tozzla, G. Vlaic, J. Catal. 158 (1996) 486.
[12] P. Selvam, S.E. Dapurkar, S.K. Badamali, M. Muragasan, H. Kuwano, Catal. Today 68 (2001) 69.
[13] Y. Kuang, N. He, J. Wang, P. Xiao, C. Yuan, Z. Lu, Colloid Surf. A 179 (2001) 177.
[14] L. Marchese, T. Maschmeyer, E. Gianotti, S. Soluccia, J.M. Thomas, J. Phys. Chem. B 101 (1997) 8836.
[15] C. Berlini, M. Guidotti, G. Moretti, R. Psaro, N. Ravasio, Catal. Today 60 (2000) 219.
[16] C.A. Parks, Chem. Rev. 15 (1965) 177.